NANO LETTERS

Letter

pubs.acs.org/NanoLett

Controlling Graphene Ultrafast Hot Carrier Response from Metal-like to Semiconductor-like by Electrostatic Gating

S.-F. Shi,*[,†,‡] T.-T. Tang,[†] B. Zeng,[†] L. Ju,[†] Q. Zhou,[†] A. Zettl,[†,‡,§] and F. Wang*[,†,‡,§]

[†]Department of Physics, University of California at Berkeley, Berkeley, California 94720, United States

[‡]Material Science Division, Lawrence Berkeley National Laboratory, Berkeley, California 94720, United States

[§]Kavli Institute at University of California at Berkeley, Berkeley, California 94720, United States

Supporting Information

ABSTRACT: We investigate the ultrafast terahertz response of electrostatically gated graphene upon optical excitation. We observe that the photoinduced terahertz absorption increases in charge neutral graphene but decreases in highly doped graphene. We show that this transition from semiconductor-like to metal-like response is unique for zero bandgap materials such as graphene. In charge neutral graphene photoexcited hot carriers effectively increase electron and hole densities and increase the conductivity. In highly doped graphene, however, photoexcitation does not change net conducting carrier concentration. Instead, it mainly increases electron scattering rate and reduce the conductivity.

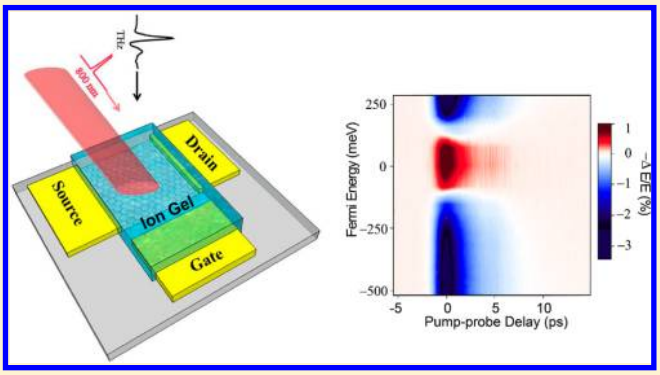

KEYWORDS: *Graphene, terahertz, hot carrier, pump−probe*

Graphene, a single layer of carbon atoms arranged in honeycomb lattice, has a linear electronic band structure with charge carriers behaving as massless Dirac fermions.[1,2] These Dirac fermions exhibit unusual electrical and optical properties. For instance, largely due to the inhibition of back scattering, the electrons in graphene have one of the highest room-temperature mobility of any material.[3−5] Optically, electrons in graphene show strong universal absorption of near-infrared and visible light from interband transitions and even stronger absorption of terahertz (THz) waves from intraband transitions.[6,7] The combination of unique electrical and optical properties makes graphene a promising candidate for future optoelectronic and plasmonic devices in particular for THz applications.[8,9] Previous studies show that optical excitation can generate "hot" charge carriers significantly out-of-equilibrium with the phonon bath in graphene,[10] which play an important role in optoelectronic responses of graphene. Understanding and further control of the dynamic response of hot carriers can potentially lead to advantageous solar cell applications exploiting carrier multiplication,[11] broad band photodetectors, and new types of hot carrier-based graphene devices.[12]

Optical pump−probe spectroscopy with various combinations of pump/probe frequency has been used to probe the transient response in interband[13,14] and intraband transition[15−21,30] in graphene. The inset of Figure 1a illustrates the microscopic process of an optical-pump THz-probe measurement of graphene in which hot electrons around the Fermi energy are generated through interband optical excitation and their effects on electrical conductivity are probed by a delayed THz probe pulse with picosecond time resolution. It has been shown[10] previously that optical excitation generates electron hole pairs that relax quickly within 100 fs and form a broadened distribution around the initial Fermi energy. This broadened Fermi distribution can be described with hot carriers of effective electronic temperature T_e. Limited by the pulse width (∼1 ps) of THz probe, optical pump-terahertz probe (OPTP) does not resolve the fast dynamics in the first 100 fs. Instead it measures the dynamic decay of the broadened Fermi distribution and provides valuable information about the hot carriers in graphene. Recently, several research groups have employed this technique to investigate transient conductivity from hot carriers in different graphene samples but observed seemingly contradictory results. George et al.[16] performed OPTP study on epitaxial multilayer graphene on SiC and found that photoexcitation leaded to a transient decrease of THz transmission that decayed fast.[16,17] However, recent OPTP study showed that optical excitation leaded to a transient increase of THz transmission in as-prepared single layer graphene grown by chemical vapor deposition (CVD) method.[18−20] For example, Tielrooij et al.[18] showed that optical excitation heated up electrons efficiently in as-prepared CVD graphene and induced a transient THz transparency. Jnawali et al.[20] found that this transient increase of THz transmission could be described

Received: December 30, 2013
Revised: February 23, 2014

   dx.doi.org/10.1021/nl404826r | *Nano Lett.* XXXX, XXX, XXX−XXX

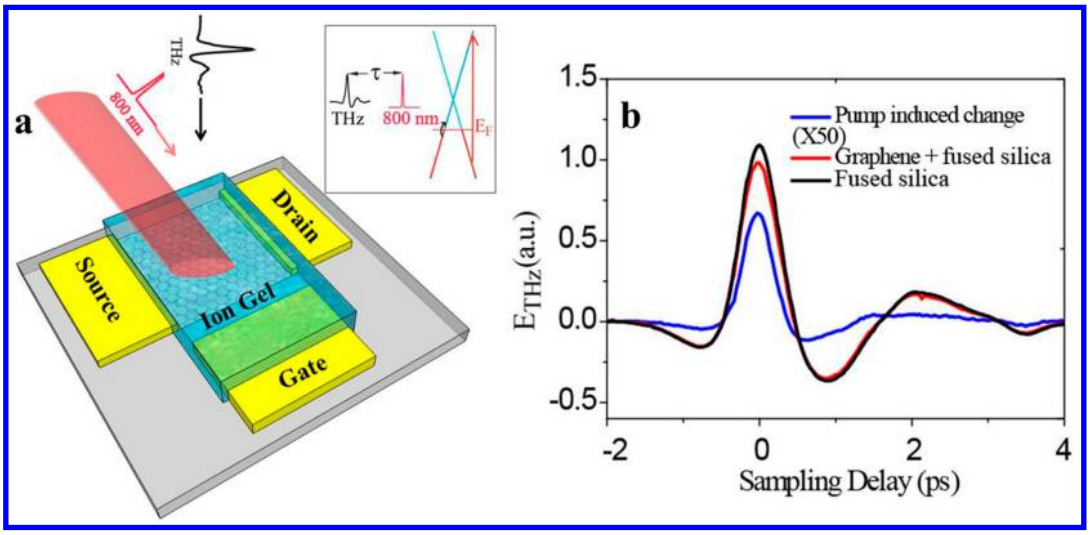

Figure 1. Optical pump THz probe spectroscopy of graphene. (a) Schematic representation of our OPTP study on a graphene FET device. THz transparent ion gel is used to efficiently control the Fermi energy of graphene. The inset shows the working principle of OPTP spectroscopy of graphene with a Fermi energy $E_F = -200$ meV (hole-doped). The inset illustrates the microscopic pump−probe process in graphene. The time delay between optical pump and THz probe beam is τ. (b) THz waveforms transmitted through fused silica substrate (black trace) and through as-prepared CVD graphene on fused silica substrate (red trace). Pump-induced change in transmitted THz waveform (at $\tau = 0$) is also displayed after a magnification of 50 times (blue trace).

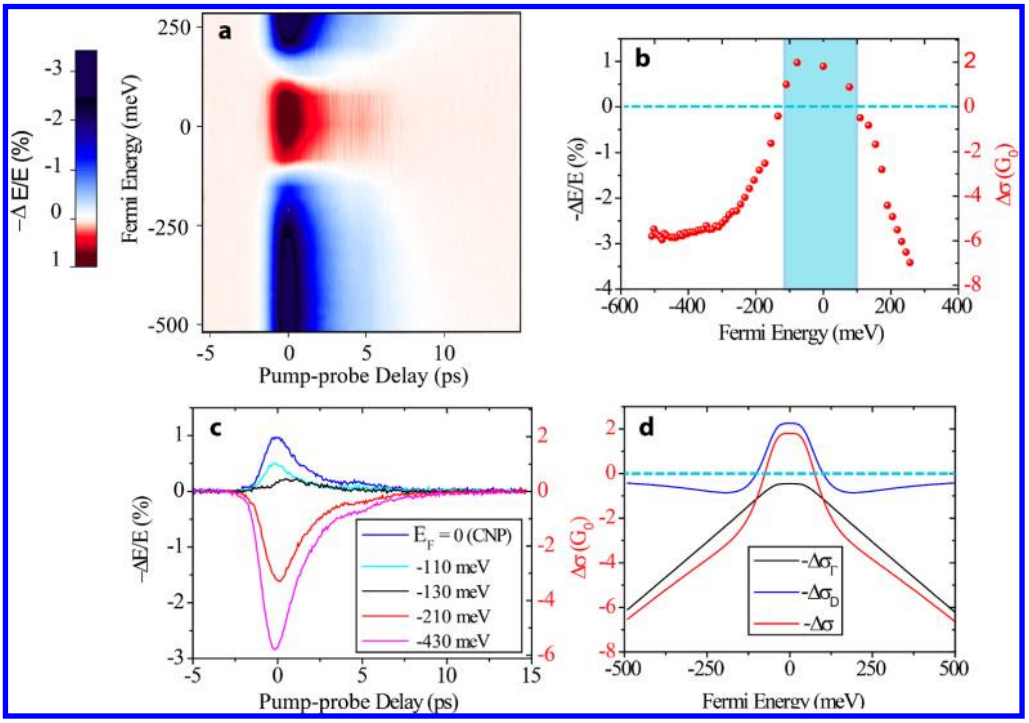

Figure 2. Controlling the hot carrier response of graphene through electrostatic gating. (a) Two-dimensional color plot of optical pump induced THz field transmission change ($-\Delta E/E$) as a function of pump delay τ and initial Fermi energy of graphene. Optical pump fluence intensity is fixed at 12.7 μJ/cm^2. (b) A vertical cut of the 2D plot at $\tau = 0$ shows Fermi energy dependence of $-\Delta E/E$, which changes sign when graphene Fermi energy is shifted away from the charge neutral point. The corresponding change in THz conductivity ($\Delta\sigma$) is shown at the right axis. (c) Horizontal cuts of the 2D plot show time evolution of $-\Delta E/E$ (left axis) and corresponding $\Delta\sigma$ (right axis) at different Fermi energies. (d) Theoretical prediction of $\Delta\sigma$ from hot carriers as a function of initial Fermi energy in graphene. We assumed a hot carrier temperature of 600 K. The total change in conductivity ($\Delta\sigma$, read trace) includes contribution from the scattering rate change ($\Delta\sigma_\Gamma$, black trace) and from the Drude weight change ($\Delta\sigma_D$, blue trace). It shows a transition from semiconductor-like behavior in charge neutral graphene (where the contribution from Drude weight increase dominates) to metal-like behavior in highly doped graphene (where the contribution from scattering rate increase dominates).

within the context of the Drude model with an increased scattering rate for hot electrons. More complicated responses were further observed in graphene exposed to different gas species, where a theory of bandgap opening was invoked to explain the data.[21] So far a complete picture of optical excitation-induced THz responses in different graphene samples is still lacking: do the different responses arise from different electronic band structures in different graphene

dx.doi.org/10.1021/nl404826r | Nano Lett. XXXX, XXX, XXX−XXX

samples, or can it be intrinsic behavior of Dirac electrons in graphene with different carrier concentrations? However, in contrast to extensive electrical transport works that utilize electrostatic gating to reveal unique Dirac fermion physics in graphene, there is no OPTP study available on electrostatically gated graphene devices so far. The challenge is that the gate electrode is often opaque to THz waves or the gate electrode has a large OPTP signal that overwhelms the graphene response.

In this work, we perform systematic OPTP spectroscopy of graphene by actively controlling the Fermi energy of graphene for the first time. We achieve this by using ion gel as efficient gating dielectrics,[22,23] which is both transparent to THz waves and optical excitation. This enables the OPTP study on graphene with actively controlled Fermi energy for the first time (Figure 1a). We observe that the photoinduced THz responses in graphene, unlike those in conventional materials, change sign with increased initial carrier concentration. This sign change in photoinduced THz absorption corresponds to a transition from semiconductor-like to metal-like response to the optical excitation at different doping. We show that this transition of behavior arises naturally in zero bandgap semiconductors such as graphene. Specifically, at charge neutral point (CNP) the THz response of graphene is dominated by an increase in conducting carrier density that increases the conductivity, whereas in highly doped graphene an increase of scattering rate dominates the THz response and decrease the conductivity. Our results provide a unifying picture that describes the hot carriers responses observed in all previous studies and also shed light on preparing optoelectronic and THz devices based on graphene.

We use time-domain THz spectroscopy (see Supporting Information[23]) to probe the transient conductivity in single layer CVD graphene on fused silica.[24] Figure 1b displays typical THz waveforms transmitted through a bare fused silica substrate (black trace) and through as-prepared graphene on a fused silica substrate (red trace). The difference in THz electrical field $\Delta E(\omega)$ is directly proportional to the frequency-dependent electrical conductivity change ($\Delta\sigma$) from the presence of graphene, which is described by[25]

$$\Delta\sigma \approx -\frac{n+1}{Z_0}\frac{\Delta E(\omega)}{E_0(\omega)} \tag{1}$$

Here $n = 1.96$ is the refractive index of fused silica from 0.3 to 1.0 THz,[26] $Z_0 = 377\ \Omega$ is the vacuum impedance, and $E_0(\omega)$ is the Fourier transform of the transmitted THz field through the fused silica reference substrate. It yields a largely frequency independent sheet conductivity of ~23 G_0 ($G_0 = e^2/h$) between 0.3 to 1 THz (see Supporting Information[23]) for as-prepared graphene. This large conductivity indicates that our as-prepared CVD graphene is significantly doped, consistent with previous reports.[6,7,20] Optical pump induced THz transmission change on the same sample is also displayed in Figure 1b after being magnified 50× (blue trace). It shows an increase of transient THz transmission, consistent with previous studies on CVD graphene[18−20] but opposite to the behavior in epitaxial multilayer graphene on SiC.[16,17] From the THz transmission increase (ΔE) in Figure 1(b) for CVD graphene, we obtain a photoinduced reduction of conductivity $\Delta\sigma \sim -3G_0$.

The photoinduced THz response in graphene, however, can change dramatically with electrostatic gating. For simplicity, we focus on the relative change in the amplitude of the THz waveform ($-\Delta E/E_0$) and plot its dependence on the pump−probe time delay (τ) and the graphene Fermi energy in Figure 2a. One salient feature in the figure is that the photoinduced THz conductivity switches signs close to the CNP, changing from positive (decreased transmission) in undoped graphene to negative (increased transmission) in highly doped graphene. Figure 2b displays a vertical line cut of the two-dimensional plot at $\tau = 0$, showing clearly that the photoinduced THz response changes sign in a window ~±100 meV away from CNP (shaded area). Figure 2c shows horizontal line cuts of the two-dimensional (2D) plot, displaying the decay of photoinduced THz response at different doping. Despite a change of sign in THz responses, the decay dynamics remains similar with a decay time of 1.9 ps at CNP and 2.0 ps for $E_F = -430$ meV. Such decay times are similar to previous studies at room temperature.[16,20]

This dramatic change in photoinduced THz response as a function of electrical doping in graphene can be attributed to the unusual hot carrier effects in a Dirac material like graphene. THz responses from hot carriers can be approximated by a Drude conductivity $\sigma \approx (D/\Gamma)$ (for $\Gamma \gg 1$ THz)[6] where Γ is the scattering rate and D is the Drude weight. At elevated electronic temperature, the change in Drude conductivity can be expressed as

$$\Delta\sigma \approx \left(\frac{\Delta D}{D_0} - \frac{\Delta\Gamma}{\Gamma_0}\right)\sigma_0 \tag{2}$$

Here D_0 and Γ_0 are, respectively, the Drude weight and the scattering rate without optical pump, and ΔD and $\Delta\Gamma$ are the optical pump induced changes. In conventional semiconductors, the conductivity increases with temperature because the change is dominated by an increase in Drude weight (through the increased conducting carrier concentration), while in conventional metals the conductivity decreases with temperature because the change is dominated by an increased electron scattering rate. In Dirac materials like graphene, which has zero bandgap, the relative contributions from the Drude weight and the scattering rate to $\Delta\sigma$ can vary significantly as a function of the initial Fermi energy; the hot carrier-induced THz responses can switch from semiconductor-like at zero doping to metal-like at high doping.

In Figure 2d, we plot a theoretical estimate of the total Drude conductivity change ($\Delta\sigma$) from hot carriers as well as the respective contribution from the scattering rate change ($\Delta\sigma_\Gamma = -(\Delta\Gamma/\Gamma_0)\sigma_0$) and the Drude weight change ($\Delta\sigma_D = -(\Delta D/D_0)\sigma_0$) for different Fermi energies. Here we have assumed values that are representative of our experimental conditions with $\hbar\Gamma_0 = 16$ meV,[6] electronic temperature $T_e = 600$ K, and $\Delta\Gamma/\Gamma_0 = 20\%$. The Drude weight in Dirac materials is described by[27]

$$D = G_0 2kT_e \ln\left[2\cosh\left(\frac{E_F}{2kT_e}\right)\right] \tag{3}$$

where E_F is Fermi energy and k is the Boltzmann constant. Figure 2d clearly shows that the contribution from Drude weight change ($\Delta\sigma_D$) dominates at the CNP, while the contribution from scattering rate change ($\Delta\sigma_\Gamma$) dominates at high doping. In particular, the theory predicts a very sensitive dependence of $\Delta\sigma_D$ on the initial Fermi energy. This behavior is characteristic of Dirac materials with zero bandgap, as we illustrate in Figure 3a. At the CNP, higher electronic

dx.doi.org/10.1021/nl404826r | Nano Lett. XXXX, XXX, XXX−XXX

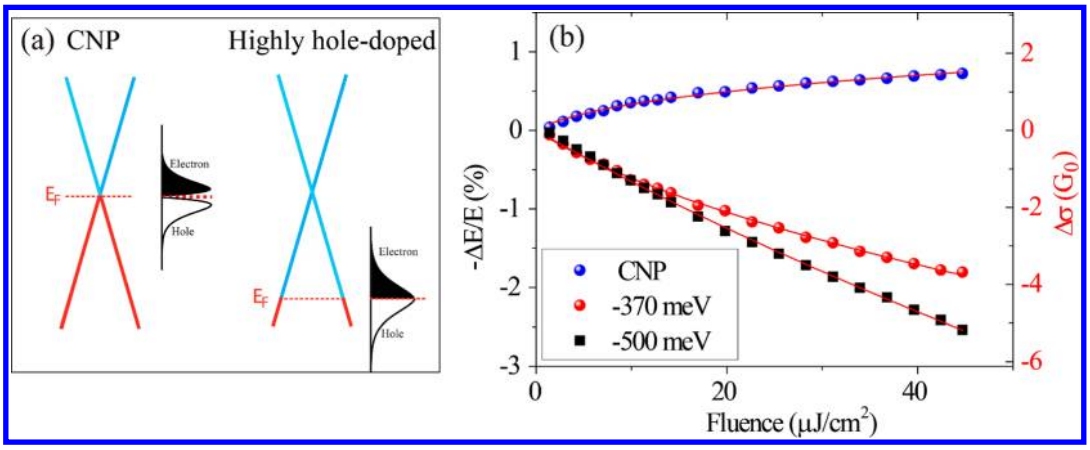

Figure 3. Fluence dependence of the hot carrier THz responses. (a) Illustration of hot carrier distribution around the initial Fermi energy for undoped and highly hole-doped graphene. At CNP, hot carriers lead to a significant increase of net charge carriers (including electrons in the conduction band and holes in the valence band). In highly doped graphene, however, hot carriers correspond to a broadening of the Fermi distribution with no net increase of charge carriers. (b) The symbols show fluence-dependent transient THz response ($-\Delta E/E$, left axis) and corresponding conductivity change ($\Delta\sigma$, right axis) in graphene at different Fermi energies. The fluence (F) dependence can be approximated by a power law at high fluence limit, scaling as $F^{1/3}$ in charge neutral graphene and as $F^{1/2}$ in highly doped graphene. Solid lines (red) show fittings from our model of hot carriers in graphene with different Fermi energies.

temperature excites both electrons into the conduction band and holes into the valence band. This dramatically increases the conducting carrier concentration and the Drude weight, as in a semiconductor. However, in highly doped graphene, higher electronic temperature mainly leads to a redistribution of charge carriers within the valence or conduction band with no net change of conducting carrier concentration. Such behavior, where the Drude weight barely changes (see Supporting Information for exact calculations[23]) upon optical excitation, is characteristic of traditional metal. A comparison between theory (red line in Figure 2d) and experiment (red dots in Figure 2b) shows that this simple hot-carrier model can reproduce all the main features in the experimental data.

We can gain further insight into hot carrier effects by examining the power dependence of the photoinduced THz responses. Figure 3b shows that the photoinduced THz response ($-\Delta E/E$, or equivalently $\Delta\sigma$) has a strong nonlinear dependence on the pump fluence, scaling with fluence in the high fluence limit as $\sim F^{1/3}$ at the CNP (blue dots) and as $\sim F^{1/2}$ at high doping. Previously, only an $F^{1/2}$ power law scaling was observed.[15,20,28,31] For our experimental conditions, $\Delta\sigma$ is proportional to the electronic temperature increase in both charge neutral and highly doped graphene (see Supporting Information[23]), and the different power law scaling of $\Delta E/E$ can be understood from the fluence dependence of ΔT_e.

Assuming a certain fraction (γ) of the incident photon energy is captured in the hot electron distribution, we can calculate the hot electron temperature T_e using the electronic heat capacity, C_e of Dirac electrons. At the CNP, $C_e = \beta T_e^2$ with $\beta = \{[(18\zeta(3)]/[\pi(\hbar v_F)]^2\}k^3(\zeta(3) = 1.202)$.[10] For highly doped graphene ($kT_e \ll |E_F|$), we have $C_e = \alpha T_e$ with $\alpha = (2\pi/3)k^2[(E_F)/(\hbar V_F)^2]$.[29] Therefore the hot electron temperature behaves as $T_e = T_0(1 + 3\gamma F/\beta T_0^3)^{1/3}$ at the CNP and $T_e = T_0(1 + 2\gamma F/\alpha T_0^2)^{1/2}$ in highly doped graphene. In the limit of high pump fluence (i.e., $T_e \gg T_0$), we obtain $\Delta T_e \propto F^{1/3}$ at CNP and $\Delta T_e \propto F^{1/2}$ at high doping, reproducing the power laws observed in the experiment. In the low fluence limit, ΔT_e is linear with pump fluence. Figure 3b shows that a fitting using the hot carrier model (solid lines) describes well the experimental data across the entire pump fluence range. In this fitting, we use a γ value of 1×10^{-3}, which corresponds to ~10% of the absorbed photon energy remaining in the hot carriers at ~1 ps after the excitation.[10] Using this information, we can also obtain the hot electron temperature for both different pump fluences and carrier concentrations (see Supporting Information[23]). Consequently, at the CNP graphene has a smaller electronic heat capacity, so a given optical excitation will heat up electrons most efficiently in undoped than doped graphene. Because our previous discussion of Drude weight also shows that hot electrons increase the density of electrons and holes as conducting carriers more efficiently at the CNP, we find that the neutral graphene should be exploited for efficient carrier multiplication.

In summary, we find that hot carriers in graphene lead to unusual transient THz conductivity response, which can be switched from a semiconductor-like response to optical excitation at the CNP to a metal-like response at high doping. At the same time, its fluence dependence changes from $F^{1/3}$ to $F^{1/2}$ as the doping is increased. Exploiting this unique and gate-tunable hot carrier response in graphene could lead to new high speed optoelectronic devices.

■ ASSOCIATED CONTENT

Ⓢ Supporting Information

Details about the sample preparation, measurement, and data analysis. This material is available free of charge via the Internet at http://pubs.acs.org.

■ AUTHOR INFORMATION

Corresponding Authors

*E-mail: (S.-F.S.) sufeishi@berkeley.edu. Tel: (510) 643-3275. Fax: (510) 486-6054.

*E-mail: (F.W.) fengwang76@berkeley.edu. Tel: (510) 643-3275. Fax: (510) 486-6054.

Notes

The authors declare no competing financial interest.

■ ACKNOWLEDGMENTS

We thank Dr. J. C. Lischner, Dr. M. W. Graham, Dr. W. Li, Dr. R. P. Smith, X. Hong, and J. Kim for helpful discussions.

Optical characterization of this work was mainly supported by Office of Basic Energy Science, Department of Energy under Contract Nos. DE-SC0003949 and DE-AC02-05CH11231. Graphene synthesis and photonic device fabrication were supported by the Office of Naval Research (award N00014-13-1-0464 and MURI N00014-09-1-1066). We also acknowledge the support from a David and Lucile Packard fellowship.

REFERENCES

(1) Novoselov, K. S.; Geim, A. K.; Morozov, S. V; Jiang, D.; Katsnelson, M. I.; Grigorieva, I. V.; Dubonos, S. V.; Firsov, A. A. *Nature* **2005**, *438*, 197−200.
(2) Zhang, Y.; Tan, Y.-W.; Stormer, H. L; Kim, P. *Nature* **2005**, *438*, 201−204.
(3) Geim, A. K.; Novoselov, K. S. *Nat. Mater.* **2007**, *6*, 183−191.
(4) Bolotin, K. I.; Sikes, K. J.; Jiang, Z.; Klima, M.; Fudenberg, G.; Hone, J.; Kim, P.; Stormer, H. L. *Solid State Commun.* **2008**, *146*, 351−355.
(5) Dean, C. R.; Young, A. F.; Meric, I.; Lee, C.; Wang, L.; Sorgenfrei, S.; Watanabe, K.; Taniguchi, T.; Kim, P.; Shepard, K. L.; Hone, J. *Nat. Nanotechnol.* **2010**, *5*, 722−726.
(6) Horng, J.; Chen, C.-F.; Geng, B.; Girit, C.; Zhang, Y.; Hao, Z.; Bechtel, H. A.; Martin, M.; Zettl, A.; Crommie, M. F.; Shen, Y. R.; Wang, F. *Phys. Rev. B.* **2011**, *83*, 165113.
(7) Ren, L.; Zhang, Q.; Yao, J.; Sun, Z.; Kaneko, R.; Yan, Z.; Nanot, S.; Jin, Z.; Kawayama, I.; Tonouchi, M.; Tour, J. M.; Kono, J. *Nano Lett.* **2012**, *12*, 3711.
(8) Avouris, P. *Nano Lett.* **2010**, *10*, 4285−4294.
(9) Ju, L.; Geng, Bai.; Horng, J.; Girit, C.; Martin, M.; Hao, Z.; Betchtel, H. A.; Liang, X.; Zettl, A.; Shen, Y. R.; Wang, F. *Nat. Nanotechnol.* **2011**, *6*, 630−634.
(10) Liu, C. H.; Mak, K. F.; Shan, J.; Heinz, T. F. *Phys. Rev. Lett.* **2010**, *10*, 127404.
(11) Gabor, N. M.; Song, J. C. W.; Ma, Q.; Nair, N. L.; Taychatanapat, T.; Watanabe, K.; Taniguchi, T.; Levitov, L. S.; Jarillo-Herrero, P. *Science* **2011**, *334*, 648−652.
(12) Vaziri, S.; Lupina, G.; Henkel, C.; Smith, A. D.; Östling, M.; Dabrowski, J.; Lippert, G.; Mehr, W.; Lemme, M. C. *Nano Lett.* **2013**, *13*, 1435.
(13) Sun, D.; Wu, Z-K; Divin, C.; Li, X.; Berger, C.; de Heer, W. A.; First, P. N.; Norris, T. B. *Phys. Rev. Lett.* **2008**, *101*, 157402.
(14) Winnerl, S.; Orlita, M.; Plochocka, P.; Kossacki, P.; Potemski, M.; Winzer, T.; Malic, E.; Knorr, A.; Sprinkle, M.; Berger, C.; de Heer, W. A.; Schneider, H.; Helm, M. *Phys. Rev. Lett.* **2011**, *107*, 237401.
(15) Li, T.; Luo, L.; Hupalo, M.; Zhang, J.; Tringides, M. C.; Schmalian, J.; Wang, J. *Phys. Rev. Lett.* **2012**, *108*, 167401.
(16) Geoge, P. A.; Strait, J.; Dawlaty, J.; Shivaraman, S.; Chandrashekhar, M.; Rana, F.; Spencer, M. G. *Nano Lett.* **2008**, *8*, 4248−4251.
(17) Strait, J. H.; Wang, H.; Shivaraman, S.; Shields, V.; Spencer, M.; Rana, F. *Nano Lett.* **2013**, *11*, 4902−4906.
(18) Tielrooij, K. J.; Song, J. C. W.; Jensen, S. A.; Centeno, A.; Pesquera, A.; Zurutuza Elorza, A.; Bonn, M.; Levitov, L. S.; Koppens, F. H. L. *Nat. Phys.* **2013**, *9*, 248.
(19) Frenzel, A. J.; Lui, C. H.; Fang, W.; Nair, N. L.; Herring, P. K.; Jarillo-Herrero, P.; Kong, J.; Gedik, N. *Appl. Phys. Lett.* **2013**, *102*, 113111.
(20) Jnawali, G.; Rao, Y.; Yan, H.; Heinz, T. F. *Nano Lett.* **2013**, *13*, 524−530.
(21) Docherty, C. J.; Lin, C.-T.; Joyce, H. J.; Nicholas, R. J.; Herz, L. M.; Li, L-J; Johnston, M. B. *Nat. Commun.* **2012**, *3*, 1228.
(22) Chen, C.-F.; Park, C.-H.; Boudouris, B. W.; Horng, J.; Geng, B.; Girit, C.; Zettl, A.; Crommie, M. F.; Segalman, R. A.; Louie, S. G.; Wang, F. *Nature* **2012**, *471*, 617.
(23) Supporting Information.
(24) Li, X.; Cai, W.; An, J.; Kim, S.; Nah, J.; Yang, D.; Piner, R.; Velamakanni, A.; Jung, I.; Tutuc, E.; Banerjee, S. K.; Colombo, L.; Ruoff, R. S. *Science* **2009**, *324*, 1312.
(25) Tinkham, M. *Phys. Rev.* **1956**, *104*, 845.
(26) Naftaly, M.; Miles, R. E. *Proc. IEEE.* **2007**, *95*, 1658.
(27) Gusynin, V. P.; Sharapov, S. G.; Carbotte, J. P. *New J. Phys.* **2009**, *11*, 095013.
(28) Graham, M. W.; Shi, S.-F.; Ralph, D. C.; Park, J.; McEuen, P. L. *Nat. Phys.* **2013**, *9*, 103.
(29) Song, J. C. W.; Reizer, M. Y.; Levitov, L. S. *Phys. Rev. Lett.* **2012**, *109*, 106602.
(30) Kim, J.; et al. *Sci. Rep.* **2013**, *3*, 2663.
(31) Dani, K. M.; et al. *Phys. Rev. B* **2012**, *86*, 125403.